Contributions to Geophysics and Geodesy Vol. 55/4, 2025 (571–601)

Aquifer potential zones within Akure, Nigeria, using geo-electrical derived parameters and GIS multi-criteria model approach

Olubunmi Oluwatoyin OMOTOLA[1], Adewale Henry OLABINTAN[2,*]

[1] Department of Geology, Olusegun Agagu University of Science and Technology, Okitipupa, Ondo State, Nigeria

[2] Department of Physics, Federal University Oye-Ekiti, Ekiti State, Nigeria

Abstract: This research addresses the recurring issue of water scarcity during dry seasons in Akure metropolis, Nigeria—a crisis exacerbated by demographic growth, increasing domestic and industrial water demands, and groundwater overexploitation. Through comprehensive geophysical investigations, we developed a methodological framework to identify and spatially delineate zones of groundwater resource prospect. Our approach integrated multiple hydrogeological parameters derived from electrical resistivity surveys (transverse resistance, hydraulic conductivity, and aquifer transmissivity) with lineament density analysis from satellite imagery to create thematic spatial representations. These parameters were systematically weighted using the Analytical Hierarchy Process (AHP) within a multi-criteria decision analysis framework to construct a groundwater prediction mapping index. The results from the iso-resistivity map of the saprolite layer revealed areas with clayey aquifers, fractured/clayey aquifers, sand/clayey sand aquifers. The isopach map of the saprolite layer shows areas with low, medium, and high groundwater yield. The depth to basement surface layer map revealed areas with bedrock swells and locations with bedrock troughs which will be suitable for groundwater exploration. The resulting groundwater potential prediction model classified the investigated site into four specific categories: low, low-medium, medium, and medium-high potential zones. The results show that nearly 92% of the metropolitan zones exhibit relatively low groundwater prospects, with only 8% demonstrating suitable characteristics for sustainable extraction. This research provides critical spatial intelligence for identifying viable groundwater development zones and serves as a guide for local water authority bodies to reduce borehole failures.

Key words: groundwater prospect mapping, analytical hierarchy procedure, hydrogeophysics, geospatial analysis, basement aquifer systems

*corresponding author, e-mail: adewale.olabintan@fuoye.edu.ng, phone: +2348036550941

doi: 10.31577/congeo.2025.55.4.8

1. Introduction

Groundwater significantly influences global climate change and meets human needs. Water-bearing formations transform into a valuable resource when they possess sufficient permeability to facilitate the infiltration of water. This enables the extraction of ample supplies of portable water through boreholes, shallow wells, and wellsprings. Additionally, these formations must be capable of being replenished by recharge sources to support ongoing utilisation. The flow of groundwater from the earth's surface into the underlying aquifers is determined by the porosity and permeability of the rocks in which the gravity effect is important (*Stigter et al., 2006*). Groundwater primarily originates from rainwater and snowmelt, flowing through the aquifer via the soil pores (*Mallick et al., 2019*).

Freshwater resources are in higher demand as a result of the global population and business growth. The shortage of water is felt by more than 40% of the global residents; if the prevailing situation continues, over 6.3 billion people will experience different types of water pressure by 2030 (*Kumar et al., 2024*). Human actions have resulted in the quality of the remaining water bodies declining over the last three decades, causing the drying of 85% of the world's water bodies (*Joleha et al., 2024*). Excessive groundwater extraction can lead to declining groundwater levels, land subsidence, salinisation, diminished well yields, elevated pumping costs, and increased saltwater intrusion (*Jaafarzadeh et al., 2021; Kumar et al., 2023*). These alterations have led to a 60% drop in the surface area of key aquifers in various regions globally (*Richey et al., 2015*).

Surface water and groundwater serve as essential resources for water supply systems and agricultural needs (*Madhav and Singh, 2021*). Despite the frequent use of surface water for supply purposes due to its accessibility and reliability, groundwater remains the dominant water source across numerous areas, especially in developing countries (*Kagabu et al., 2013; Kooy, 2014; Kumar et al., 2021*). Groundwater development is often cost-effective in the long run, has minimal pollution levels, and is readily controllable by the local population (*Sikah et al., 2016; Gupta et al., 2022*).

The assessment of water-bearing areas combines quantitative and qualitative approaches to determine an area's capacity for groundwater resources by analysing various indicators. Underground information is collected using monitoring wells, electrical resistivity surveys, and field examinations,

whereas surface characteristics are identified through remote sensing technology and on-site validation procedures.

Electrical resistivity techniques effectively locate potential groundwater reservoirs and water-bearing formations underground. These methods provide valuable data for estimating bedrock depth, mapping aquifers, and identifying geological structures (*Ademilua and Eluwole, 2013*). Direct-current electrical resistivity (ER) has proven most valuable among various approaches used in groundwater investigations (*Sharma and Biswas, 2013*). The distinctive advantage of ER in hydrogeophysical studies stems from its dual ability to map subsurface geological strata while simultaneously characterizing the composition of concealed underground geological units (*Hinnell et al., 2010; Fitterman et al., 2012; Kumar et al., 2020*). Additionally, strong correlations exist between the analysed ER's attributes and the actual electrical conductivity attributes of the underlying materials. ER's adaptability is shown by practical applications in groundwater research, including identifying productive aquifers and assessing water transmission qualities in these subsurface reservoirs (*Oborie and Udom, 2014; Mogaji, 2016a; Mogaji and Omobude, 2017*). From geoelectrical data, researchers have evaluated aquifers' properties from the geoelectric parameters constructed in permeable media (*Ekwe et al., 2006, Singh et al., 2021*). Through a thorough investigation of geoelectric observations and inferred hydrological attributes across the investigation area, researchers have identified specific Vertical Electrical Sounding (VES) sites that can facilitate the development of effective underground water extraction systems.

The investigated site features the Basement rocks, the saprolite layers, and deep-seated fractures in the foundation rocks, which are targets of interest for aquifer water extraction (*Ayuk et al., 2013*). The water-bearing formations within the hard rock region are categorised as artesian and phreatic aquifers, making them viable for storing subsurface water (*Mogaji, 2017*).

The combination of Remote Sensing and Geographical Information Systems has been efficient in developing groundwater potential areas. The analytical hierarchy process (AHP) is employed to construct identical repositories for weighted decision analysis by applying weights to spatial data layers and categorising relevant derived classes (*Paul et al., 2020, Pajock et al., 2023; Kumar et al., 2024*), geospatial analysis and satellite imaging techniques were applied in generating the map for the groundwater occurrence.

This map classifies aquifer yield into four unique categories, ranging from low to low-medium to medium to medium-high levels. The development of this map is based on the examination of input data, with a particular focus on transverse resistance, hydraulic conductivity, aquifer transmissivity, and lineament density. The data layers and geographic features were allocated weights according to expert assessments and site-specific circumstances, illustrating their significance to groundwater potential. A map was subsequently generated utilising a weighted spatial modelling system.

The decision-making framework is a widely utilised approach for weighted decision-making, effectively applied across various domains, including ecosystem management, environmental appraisal, and territorial planning. Numerous studies have employed weighted decision analysis to determine the relative importance of thematic parameters (*Omotola et al., 2019; Mallick et al., 2019*).

This research aims to apply geo-electrical derived parameters, satellite imaging data, and spatial information system model approaches to appraise the prospective zones of aquifer resources in Akure metropolis, southwestern Nigeria. Other specific objectives include the selection of suitable sites of the zones to guide borehole drilling and, subsequently, mapping the depths and thicknesses of selected aquifers. A resistivity survey was employed in this investigation to delineate tectonic faults or cracks that may facilitate the aggregation of hydrogeological potential (*Eluwole et al., 2020*).

2. Regional setting and geological framework

2.1. Geographic context

Geologically, Nigeria falls into two district subdivisions: the basement complex and sedimentary areas. Sedimentary areas of Nigeria comprise a central and east–southern block stretching from the Atlantic Ocean to the River Benue, a middle block in the basin of the River Niger, and two Northern blocks, one in the northwest and the other in the northeast. The hard rock region currently occupies more than half of the country's entire surface area (*Ishola et al., 2023*), consisting of a central northern block and western and eastern blocks along the eastern border.

Akure Metropolis, the primary investigation site, is located within the southwestern Nigeria basement complex and situated at coordinates 07° 09′

to 07° 19′ North and 05° 07′ to 05° 17′ East in southwestern Nigeria (Fig. 1). Encompassing approximately 340 km^2 of land area, the urban region is characterised by subtle topographic variations, with terrain height profiles ranging between 260 and 470 metres above sea level. The landscape features gently rolling plains punctuated by distinctive geological formations, including isolated hills and inselbergs that rise above the surrounding terrain. Hydrologically, the area exhibits a dendritic drainage network pattern typical of regions with relatively homogeneous underlying lithology. Climatological data indicate substantial precipitation, with annual rainfall accumulation varying between 1500–2100 mm, according to the Agro-Climatological and Ecological Project (*ACEP, 2006*).

2.2. Lithological framework

The geological foundation beneath Akure Metropolis comprises four distinct petrological units belonging to the Basement region of Southwestern Nigeria (*Salako et al., 2019*) (Fig. 2). Granite gneiss constitutes the predominant lithology, extensively distributed throughout the southern and central sectors, with additional occurrences in the northwestern portions of the study area. Charnockitic formations are localised primarily within the northwestern region, while porphyritic granite bodies emerge across the

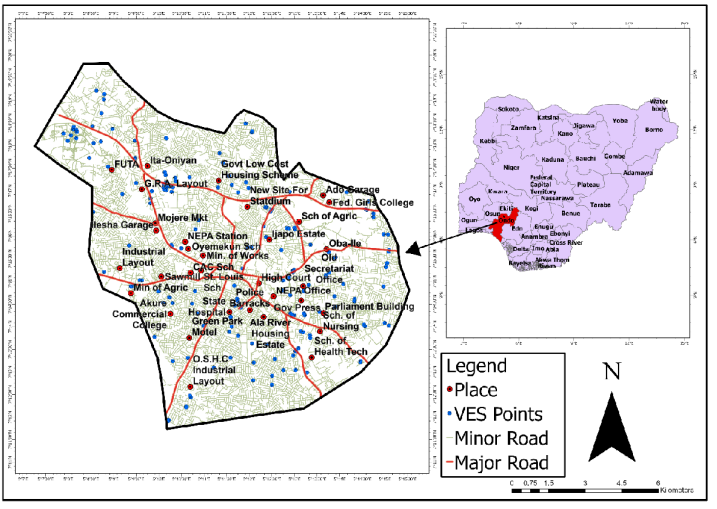

Fig. 1. Study area map illustrating the sites of VES data acquisition.

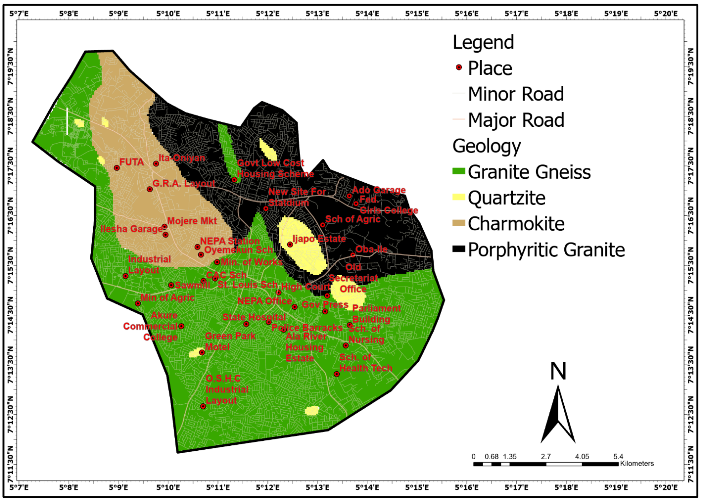

Fig. 2. The research area's geological representation (adapted from *Nigerian Geological Survey Agency (Establishment) Act, 2006*).

northeastern and central districts. Quartzite formations are concentrated within the north-central zone. The prevalence of granite gneiss throughout much of the metropolitan area has a significant influence on the region's hydrogeological characteristics.

2.3. Structural features

A vast network of structural discontinuities characterises the basement complex underneath the studied region. These include numerous fracture systems of varying dimensions, joint patterns, and fissure zones that predominantly display a north-south orientation. These structural lineaments align with the principal fracture directions previously documented throughout the Nigerian Basement Complex by *Oluyide (1988)*. These features potentially serve as significant conduits for groundwater movement within low-permeability crystalline basement rocks.

3. Methods and instrumentation

The resources employed in this research include acquired field geophysical data and remote sensing data. Figure 3 illustrates the incorporated instru-

mentation flow chart for generating the groundwater prediction map for the research area. The layer thickness (h) and layer resistivity (ρ) were generated from the iterated ER values, and the Dar-Zarrouk parameters (transverse resistance, hydraulic conductivity, and aquifer transmissivity) were constructed by evaluating the geophysical parameters. The aquifer transmissivity, hydraulic conductivity, and transverse resistance maps were created by applying spatial analysis techniques on the Dar-Zarrouk parameters. Remote sensing data from Landsat 8 imagery was utilised to generate the lineament density map. Table 1 shows information on the data collections employed for the groundwater model. The next stage involves implementing the AHP-MCDA to model groundwater prediction conditioning factors for the groundwater prediction mapping index (GWPMI). The GWPMI model created for the research was used to create a groundwater potential prediction map (GWPPM) for the examined location.

Table 1. Data collections of the groundwater model map.

Results Type	Components of the Data	Template	Output Layer
Geophysical Data	Geophysical survey carried out in the research site	Point	Transverse Resistance (TR)
Geophysical Data	Geophysical survey carried out in the research site	Point	Hydraulic Conductivity (K)
Geophysical Data	Geophysical survey carried out in the research site	Point	Aquifer Transmissivity (T)
Geospatial Imagery	Landsat 8 data	Satellite Image	Lineament density (L)

4. Data analysis and discussion

4.1. Geophysical measurements

The ER method was used to generate the 1D resistivity imaging data. In order to create the VES curves and determine the quantity, thickness, and apparent resistivity values of subsurface geological layers for both overburden materials and the aquifer unit, a total of 279 VES data points (Fig. 4) were gathered within the research area, processed, and interpreted using

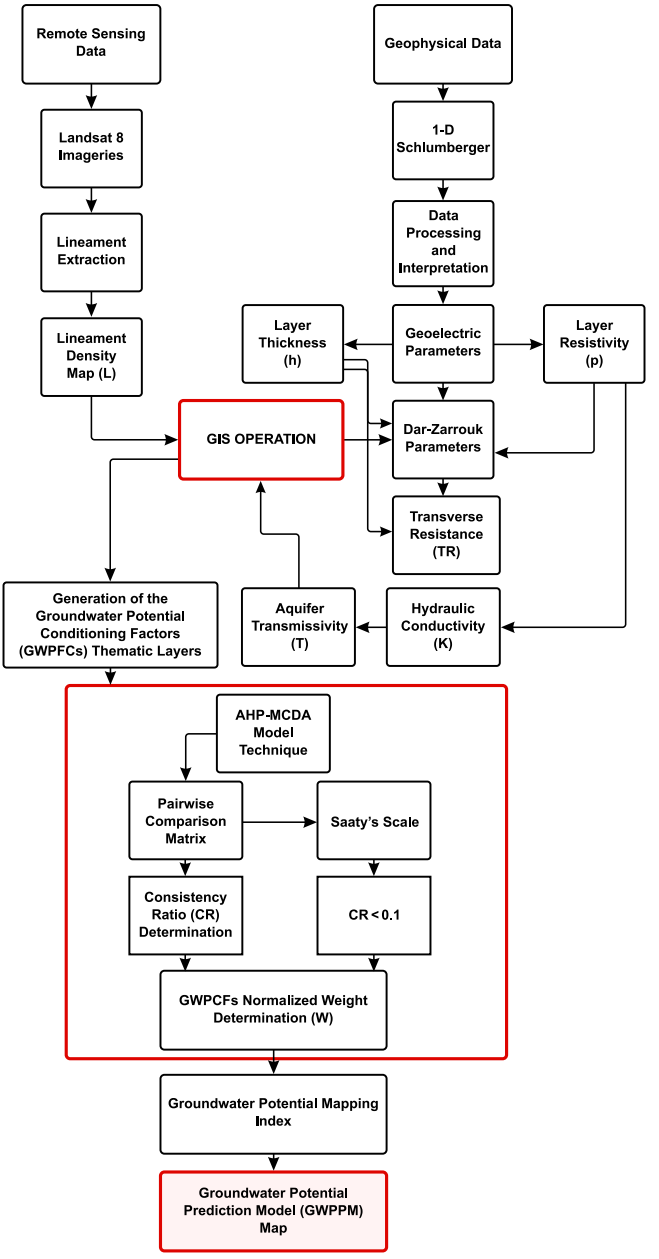

Fig. 3. Methodology flow chart of the investigated site.

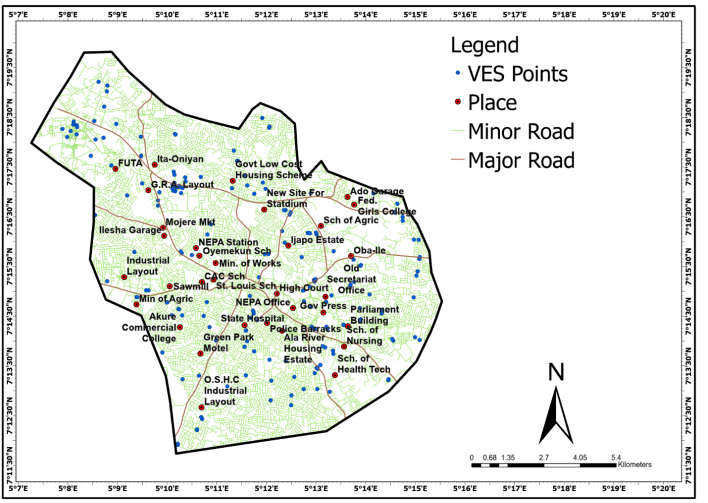

Fig. 4. The VES locations of the research site.

Win RESIST software.

Figure 5a-d illustrates the standard depth-sounding curves within the research region. The research identified fifteen curve types: H, A, K, Q, KH, HA, QH, HK, AA, AK, QK, KHK, HKH, KQH, and KHKH. The curve types vary from a basic three-layer configuration to an intricate six-layer arrangement, indicating diverse weathering, fracture, and geological sequences across the studied region (*Adelusi, 2009*). The VES locations in the investigated site are displayed in Table 2. Other curve types (such as KH, HA, HKH, KQH, etc.) suggest fractured layer aquifers, whereas the H-type curves indicate weathered layer aquifers (*Olorunfemi and Fasuyi, 1993*). In the research region, the H-type curve accounts for 35.1% of the total, while the KH-type curve accounts for 24.4%, the HK-type curve for 22%, the HKH-type curve for 4.7%, and the HA-type for 7.2%. The A-type curve exhibits 8.6%. With a succession of topsoil, worn layer, and complete bedrock, the type-H curves showed notably varying degrees of weathering across the region and stratigraphic unit. The Type-A curves indicate that the underlying geology has lower permeability and greater resistance. The study site's curve type distribution is displayed in Fig. 6. Due to the low permeability and porosity of the underlying young bedrock, the considerable predominance of these curve types indicates that most rocks acquire

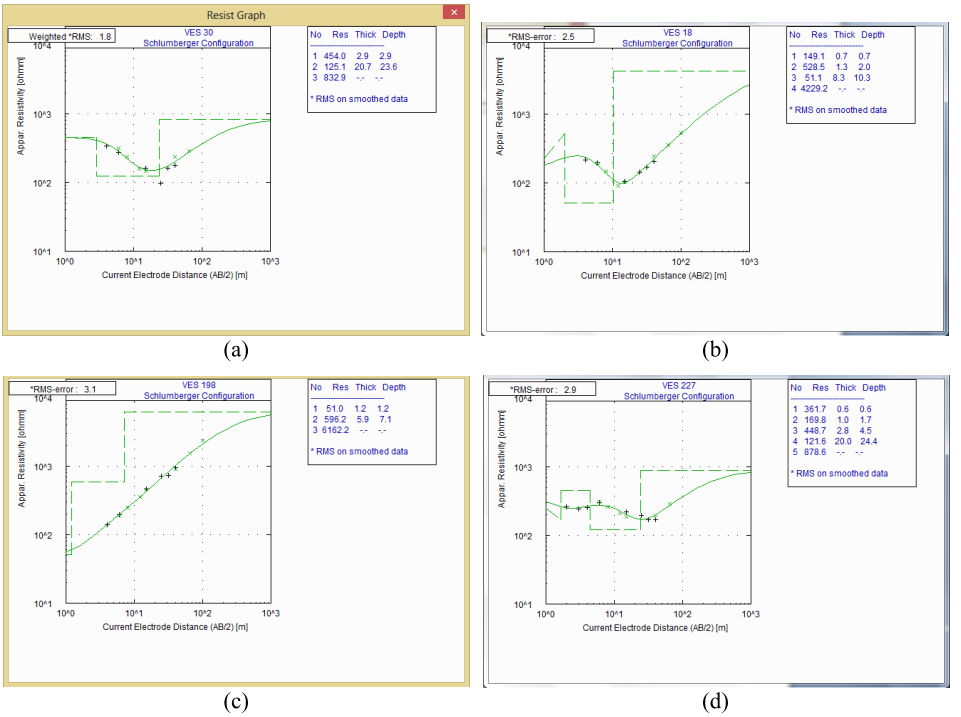

Fig. 5. (a) H sounding curve showing 3 layers: (b) KH sounding curve with 4 layers displayed: (c) a sounding revealing 3 layers: (d) HKH sounding curve showing 5 layers.

secondary porosity at a very slow rate, resulting in insufficient groundwater potential (*Mogaji et al., 2011*). The physical characteristics of each lithological unit with regard to groundwater potential at a particular location can be interpreted using these curve types, which often mirror the consecutive lithologic sequence (*Adeoye-Oladapo et al., 2015; Mogaji, 2016b*). According to *Olorunfemi and Fashuyi (1993)*, the aquifer types are comparable to those found in basement terrain in other places. In basement terrains, the regions with heavy overburden covering fragmented segments have the maximum groundwater production. Comparatively low resistivity values are mainly used to describe the areas (*Olorunfemi and Fasuyi, 1993*). The sounding curves allowed for the identification of up to four geological units. These include weathered layer, a lateritic/weathered layer, topsoil, and a fresh/fractured foundation. With layer resistivity results ranging from 6.1

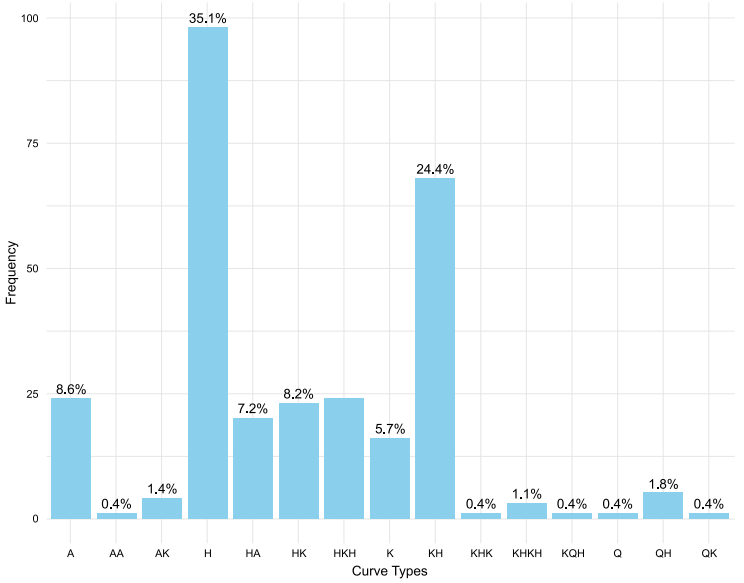

Fig. 6. Curve types distribution of the research site.

to 1960.1 Ωm, the topsoil thickness ranges from 0.3 to 8.5 metres. The average resistivity is 350.1 ohm-metres, and the average thickness is 1.2 metres.

4.1.1. The saprolite layer

A thick layer in the saprolite layer (weathered layer) may provide more storage capacity for water. A thick layer can result in the formation of subsurface features such as aquifers. The thickness of the saprolite layer also affects the rate of groundwater recharge. In the basement complex region groundwater occur in saprolite layer or in fractured/joint in the un-weathered layer (*Bello et al., 2025*). The isopach map (Fig. 7) of the saprolite layer shows the thickness of the layer. It ranges from 1.2 – 112 m. The layer's thickness is more pronounced at the central, northwestern, north central, and eastern regions of the research area. From the analysis (Table 3) generated from the isopach map using *Abiola et al. (2009)* rating, 53.5 km^2 (41%) of the study area has a thickness less than 10 m, depicting zones of low groundwater yield. 69.7 km^2 (54%) of the research area have thickness varying from 10 – 25 m representing medium groundwater yield and 6.1 km^2 (4.7%)

Table 2. VES results summary. The full listing of VES results is provided in Table S2 in a separate 'Supplement material' file).

VES No.	Easting	Northing	Resistivity (Ωm)	Thickness (m) $h_1/h_2/h_3...h_{n-1}$	AR (Ωm)	AT (m)	DB (m)	Curve Type
1	737149.2	806620.7	159.5/288.9/80.4/ 394.1	0.7/4.7/17.4	80.4	17.4	22.8	KH
2	735733.6	808131.8	116.3/19.4/818.4	2.6/7.8	19.4	7.8	10.4	H
3	735874.6	808036.8	232.4/159.6/1780/ 775.3	1.0/2.5/3.2	159.6	2.5	6.7	HK
4	737737.5	805513.6	248.7/149.8/3804.8	0.9/10.6	149.8	10.6	11.5	H
5	735855.9	808106.2	301.6/572.8/346.4/ 690.5	1.0/6.1/15.4	346.4	15.4	22.5	KH
6	735633.6	807888.8	127.5/64.1/ 1745.1	0.8/5.7	64.1	5.7	6.5	H
7	743798.4	803661.5	291.5/65.5/ 1883.4	0.8/7.1	65.5	7.1	7.9	H
8	736558.6	807582.8	338.9/165.8/1760.8 /488.6/2101.1	1.0/3.6/13.4/ 24.9	488.6	24.9	4.29	HKH
9	735633.6	807888.8	72.0/1523.8/236.7	1.3/15.4	236.7		16.7	K
10	736852.8	807645.7	162.8/231.3/947.9	0.5/21	231.3	21	21.6	A
⋮								⋮
271	738088	806832.1	4.7/36/523.9	1.8/2.8	523.9		4.5	A
272	738531.8	806180.4	40.8/186.7/54.4/ 254.6	0.7/4.8/14.1	54.4	14.1	19.6	KH
273	738089.6	805099.7	66.5/11.9/130.9	0.4/3.5	130.9		3.9	H
274	739837.9	804949.9	21.2/19.2/1384	1/4.8	19.2	4.8	5.8	H
275	739421.9	805074	42.7/226/43.5/ 957.8	0.7/3/9.9	43.5	9.9	13.6	KH
276	739135.3	805415.5	121.9/53.3/291.5	8.5/16.5	53.3	16.5	25	H
277	738717.3	805963.4	32.1/95.2/220	1.3/6.7	220		7.9	A
278	739237.8	805928.2	37.2/424.8/237.6	0.7/6.6	237.6		7.3	K
279	739681.5	805525.5	35.9/54/141.2	1.2/12.7	141.2		13.9	A

Legend: AR = Aquifer Resistivity; AT = Aquifer Thickness; DB = Depth to Bedrock.

have thickness above 25 m showing high groundwater yield. The weathered layer's iso resistivity map is shown in Fig. 8. The range of values is 14 – 684 Ωm. The findings indicate a clayey aquifer with resistivity ranging from 14 to 80 Ωm over an area of 2.5 km^2 (1.95%). The resistivity of 3.97 km^2

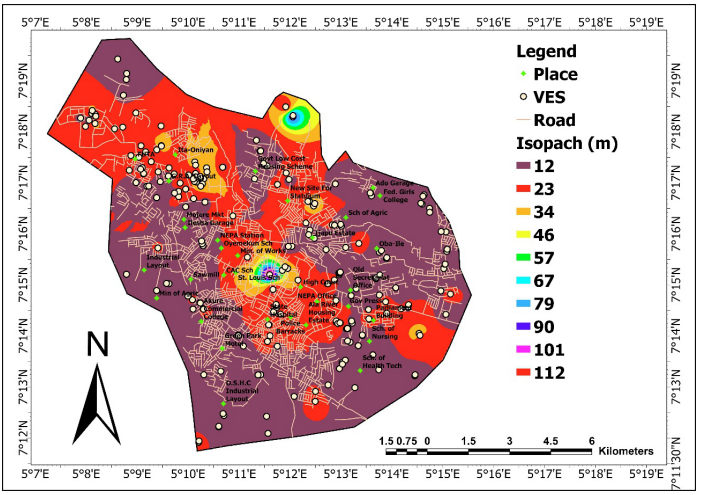

Fig. 7. Isopach map of the aquifer layer in the research site.

(3.1%) ranges from 80 to 100 Ωm, indicating a clayey or fractured aquifer. 89% of the study area, or around 115 km^2, has resistivity values between 100 and 300 Ωm. For groundwater exploration, this shows a weathered area of sand or clayey sand that is permeable and porous.

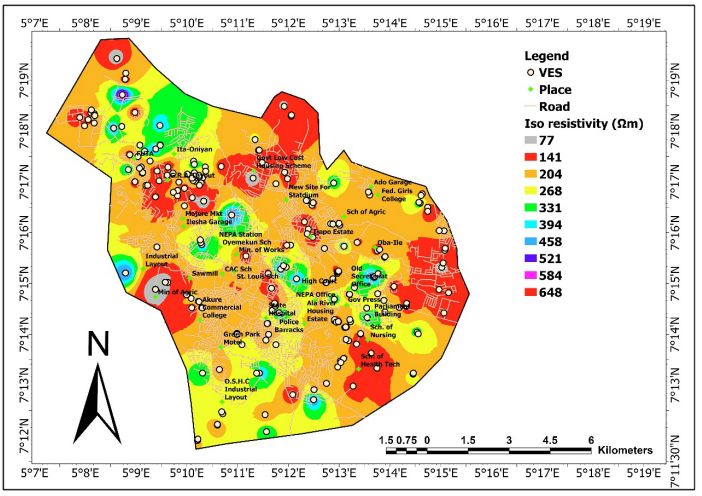

Fig. 8. Iso resistivity map of the aquifer layer in the research site.

4.1.2. The saprolite layer

The depth to the bedrock is indicated by the thickness of the overburden between the earth's surface and the basement surface (*Niaz et al., 2016*). The structural basement highs (crests) represent thin and shallow basement cover. The structural basement lows (troughs) are more suitable for groundwater reservoirs. The fragmented or fresh bedrock exhibits resistivity values between 4 Ωm to infinity (Table 2), with the depth to the basement bedrock varying from 2.6 to 147 metres. The results from the bedrock relief map (Fig. 9) show that the southern, northwestern, north eastern, western parts, and some central locations have bedrock thickness between 2.6 and 14.9 m covering an area of 56.8 km^2 (44%) (Table 3). This shows a swell in the bedrock. Most parts of the central locations, north western, north central portions and eastern flanks have thicknesses ranging from 15 – 147 m, showing a bedrock trough allowing aquifer accumulation. It covers an area of 72.2 km^2 (56%) (Table 3) of the study area. Borehole siting and water resources development would be viable in areas with a bedrock depression trough, as shown from similar studies in the Nigerian basement terrain (*Salako et al., 2019; Bello et al., 2025*).

Table 3. Analysis of the isopach, iso resistivity and bedrock relief maps.

Isopach (m)	Area (km^2)	Percentage
1.20 – 10.00	53.350185	41.36
10.01 – 25.00	69.51276	53.89
25.01 – 111.99	6.14196	4.75
Total	129.004905	100.00
Iso resistivity (Ωm)	Area (km^2)	Percentage
14.00 – 80.00	2.515995	1.95
80.01 – 100.00	3.966083	3.07
100.01 – 300.00	115.158408	89.27
300.01 – 647.85	7.383269	5.72
Total	129.023755	100.00
Bedrock Relief (m)	Area (km^2)	Percentage
2.6 – 14.9	56.801784	44.01
15.0 – 146.7	72.231532	55.99
Total	129.03	100.00

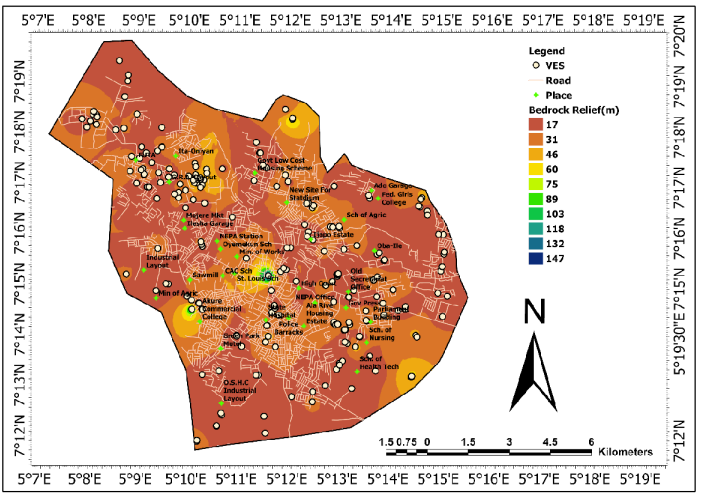

Fig. 9. Depth to basement surface relief map of the research site.

4.2. Geophysical results

Geophysical data were obtained by deploying the Vertical Electrical Soundings technique (Fig. 5a-d). Two geo-electrical attributes [resistivity (ρ) and thickness (h)] were generated from the delineated overlying and aquifer layers generated at each VES location from the interpreted results. The geo-electrical characteristics were used to determine the Dar-Zarrouk parameters. The groundwater potential modelling parameters are explained in the following subsections:

4.2.1. Transverse resistance (TR)

The transverse resistance values were derived from the Dar-Zarrouk attributes. A column cut orthogonal across the stratigraphic boundary of the sequence of strata with resistivity (ρ_n) and thicknesses (h_n) is used to estimate the aggregate transverse unit resistances, which is the definition of transverse resistance given by *Karim et al. (2013)*. The equation below represents the transverse resistance (Tr) for n layers of the identified underlying lithologies:

$$\mathrm{Tr} = \sum_{i=1}^{n} \rho_i h_i = \rho_1 h_1 + \rho_2 h_2 + \ldots + \rho_n h_n \,, \tag{1}$$

where h and ρ represent the thickness and resistivity attributes of each stratum overlaying the delineated hydrogeologic unit. Table 4 shows an analysis of the transverse resistance values.

4.2.2. Aquifer transmissivity (T)

Kaliray et al. (2014) defined aquifer transmissivity as the rate of aquifer outflow per square area. An area transmissivity parameter was determined using a mapped saturated deposit's permeability and porosity characteristics (*Ugada et al., 2014*). The geoelectric characteristics acquired at each 1D electrical resistivity imaging location from the analysed data were computed to infer the aquifer transmissivity values. Using the pertinent groundwater equation from *Khan et al. (2002)* and *Neshat et al. (2014)*, the area's transmissivity values were determined.

$$\mathrm{T} = \mathrm{K} \times h\,. \tag{2}$$

T represents the formation aquifer transmissivity, K represents the formation hydraulic conductivity, and h illustrates the aquifer thickness from the analysed field results. Table 4 shows the results of the generated aquifer transmissivity values.

4.2.3. Hydraulic conductivity (K)

The capacity of a rock material to conduct fluid under a hydraulic gradient unit is known as hydraulic conductivity (*Sattar et al., 2016*). The geoelectric parameters inferred at each 1D electrical resistivity imaging location from the processed data were also used to calculate hydraulic conductivity (K) values (Table 4). *Singh (2005)* states that the following is the non-linear connection between aquifer resistivity (ρ) and hydraulic conductivity (K):

$$\mathrm{K} = 0.0538\,\exp(0.0072\,\rho)\,, \tag{3}$$

where ρ equals the aquifer resistivity of the aquifer unit. In the works by *Adepelumi et al. (2006)*, *Mogaji et al. (2011)*, and *Omotola et al. (2019)*, the equation was used to address hydrogeological issues in the rock terrain of the Crystalline Basement with favourable outcomes. In a spatial analytic context, the inverse distance weighted approach was used to obtain the theme maps because it assumes that points closer to each other are more similar than those farther away.

Table 4. The interpreted geoelectric and Dar-Zarrouk parameters results (selected listing), the full listing is provided in Table S4 in a separate 'Supplement material' file).

VES No.	Easting	Northing	Tr (Ωm^2)	K (m/day)	T (m^2/day)
1	737149.2	806620.7	2868.44	0.918547	0.000700
2	735733.6	808131.8	302.38	0.061865	0.482546
3	735874.6	808036.8	232.40	0.169761	0.424403
4	737737.5	805513.6	223.83	0.158196	1.676875
5	735855.9	808106.2	3795.68	0.651550	10.03386
6	735633.6	807888.8	102.00	0.085353	0.486511
7	743798.4	803661.5	233.20	0.086218	0.612144
8	736558.6	807582.8	24530.5	1.813826	45.16426
9	735633.6	807888.8	23560.12	0.295750	0.000700
10	736852.8	807645.7	81.40	0.284472	5.973904
⋮					⋮
274	739837.9	804949.9	21.10	0.061776	0.296524
275	739421.9	805074.0	707.89	0.073587	0.728515
276	739135.3	805415.5	1915.60	0.438813	0.000700
277	738717.3	805963.4	679.57	0.262244	0.000700
278	739237.8	805928.2	2829.72	0.297672	0.000700
279	739681.5	805525.5	728.88	0.148697	0.000700

4.3. Remote sensing result

4.3.1. Lineament map

According to *O'Leary et al. (1976)*, lineaments are any discernible geomorphic linear feature that may be linked to lithological contacts or geological structures, particularly fractures. Lineaments provide reliable information concerning underlying geological fissures, tectonic activities, and potential natural resources of a region that are favourable for the aggregation of aquifers. Weak zones, fractures, fissures/joints, and likely weathered formations are all represented by zones of lineament occurrence (*Chowdhury et al., 2009*). ArcGIS Map was used to create the lineaments map. The lineament distribution of the investigated site is shown in Fig. 10.

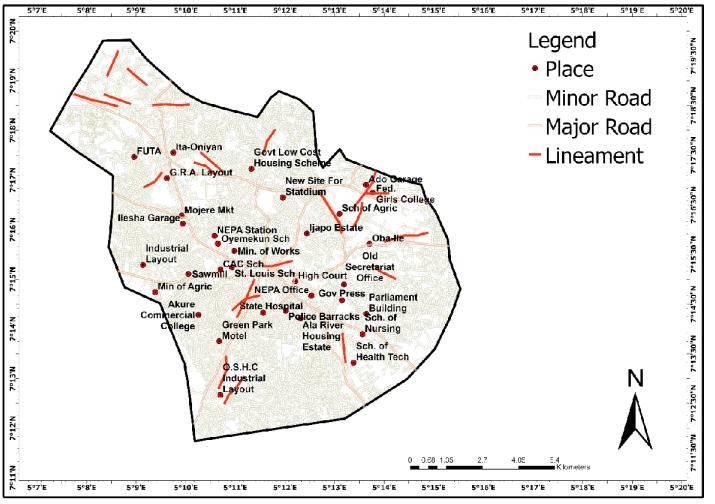

Fig. 10. Lineament distribution map of Akure metropolis.

4.3.2. Lineament density map

The ratio of all digitised lineaments to the region in question is known as the lineament density (*Edet et al., 1996*). High groundwater potential is observed in regions with high lineament densities, as demonstrated in research conducted by *Omotola et al. (2020)*. The lineament map was transformed into a quantitative model to create the lineament density map for the study region. Equation (4) shows how the lineament density (Ld) of the study area is calculated and adjusted using the inverse distance weight (IDW) estimate technique based on the cumulative length of all lineaments in each grid (*Biswas et al., 2013; Aladejana et al., 2016*).

$$\mathrm{Ld} = \sum_{i=1}^{i=n} \mathrm{L}_i / A\,, \tag{4}$$

L_i represent the cumulative length of all lineaments (km) and A is the square of the grid (km^2).

4.4. GIS tools application

4.4.1. Generation of the groundwater prediction conditioning factors (GWPCFs)

The study examined how well GIS methods could quantitatively and geo-

graphically evaluate the important contributions of groundwater prediction conditioning factors (GWPCFs) in the area under investigation. These attributes are a collection of conditioning variables that affect and regulate seepage circulation within an underlying aquifer. The geoelectric data (Table 2) and remote sensing findings were analysed within a GIS context to produce thematic maps of transverse resistance (Tr), aquifer transmissivity (T), hydraulic conductivity (K), and lineament density (L) (Figs. 11–14). The produced theme maps of the GWPCFs were then transformed into a criteria map (Fig. 15). The resulting maps were used as entry indices for creating the groundwater prediction map. Figures 11–14 illustrate the spatial characteristics of these factors in relation to groundwater occurrence assessment.

A groundwater potential model map with improved accuracy and dependability in the area was produced using the ideas and theories of AHP-MCDA. The Multi-Criteria Decision Analysis (MCDA) methodology's Analytical Hierarchy Process (AHP) technique can be employed to weight the map strata, reflecting their relative importance (*Biswas et al., 2012; Mogaji et al., 2014*). This technique was utilised to generate the weight of the Groundwater Prediction Model (GWPM) map.

In assessing the hydrological importance of these factors in the area, each

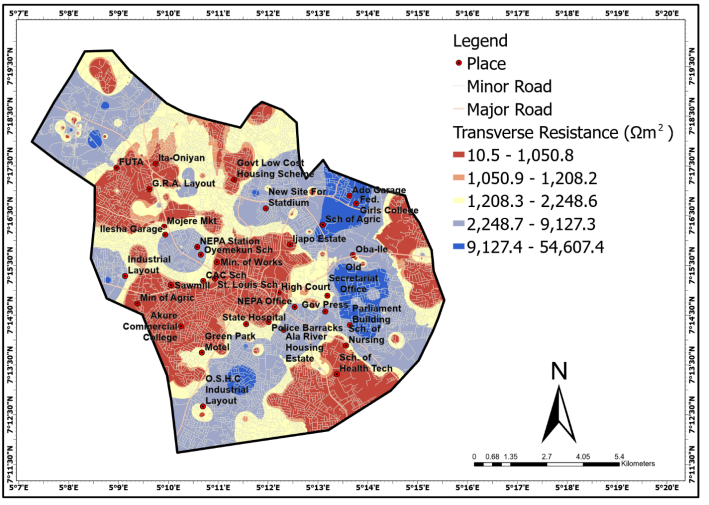

Fig. 11. Map of the investigated site's transverse resistance.

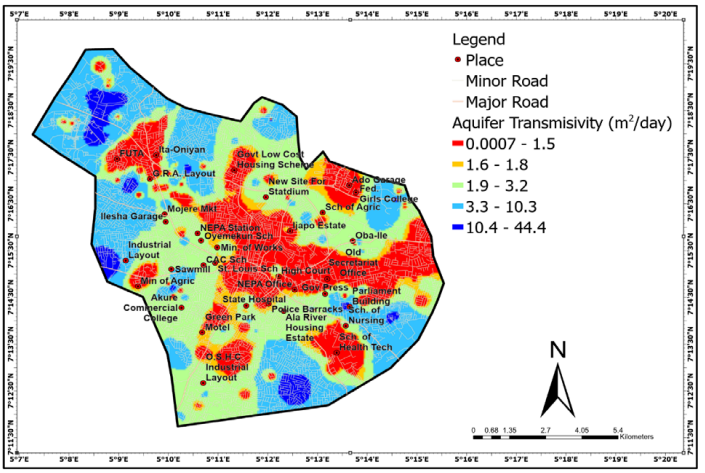

Fig. 12. Map of the investigated site's aquifer transmissivity.

factor is weighted to accurately reflect its relative importance to groundwater accumulation based on its unique hydraulic properties, which affect an aquifer's natural water flow and response to fluid extraction. Consequently, lineament density (L) is deemed the most critical characteristic, since substantial overburden materials cover the research area, and regions

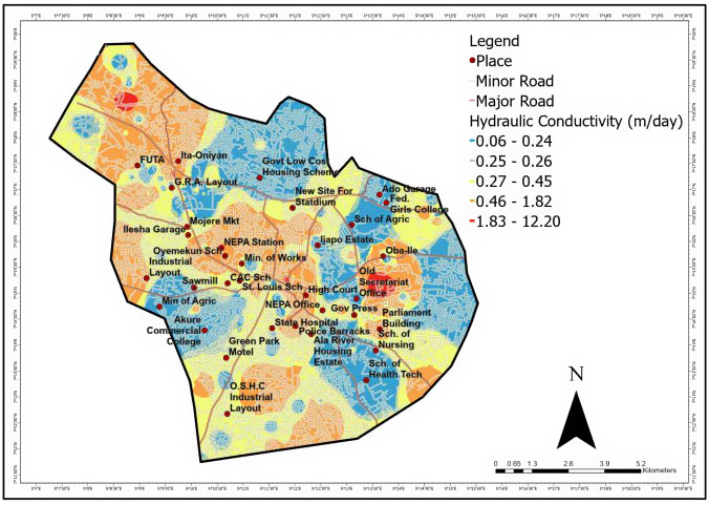

Fig. 13. Map of the investigated site's hydraulic conductivity.

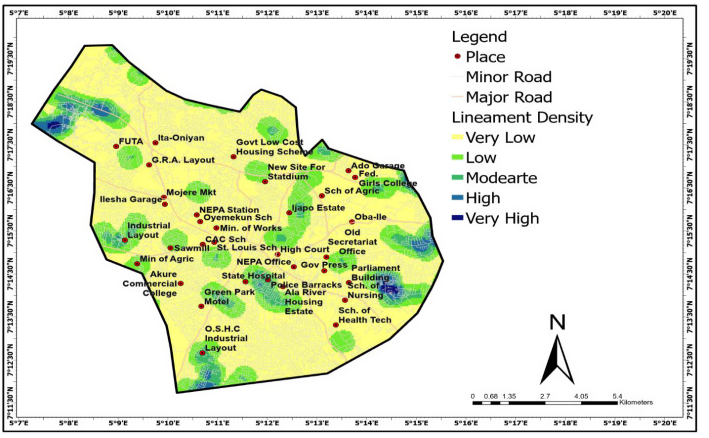

Fig. 14. Map of the investigated site's lineament density.

with considerable groundwater accumulation will be regarded as having high groundwater yield.

The Analytic Hierarchy Process (AHP) was employed to determine the weights of the four Groundwater Protection Criteria Factors (GWPCFs) by developing a pairwise comparison matrix using a standard Saaty scale, which ranges from 1 to 9 (Table 5). This involves evaluating two elements

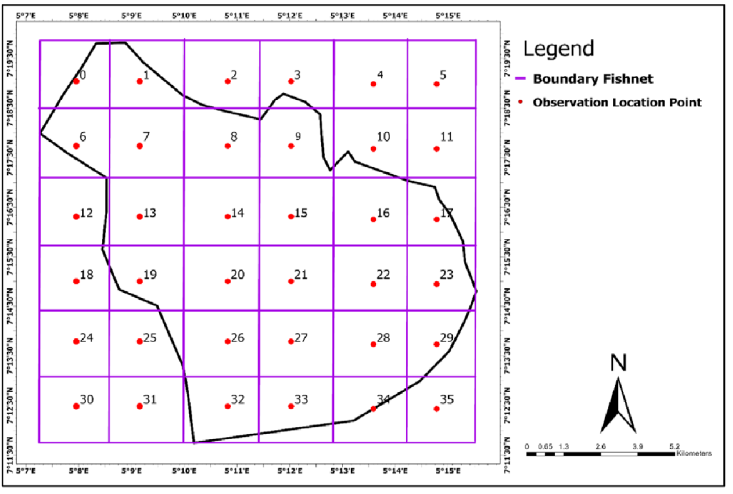

Fig. 15. Criterion map showing the grid points in the investigated site.

Table 5. AHP Technique scale and explanation.

Less Significant				Equally Significant	More Significant			
Extr	VStr	Str	Mod		Mod	Str	VStr	Extr
1/9	1/7	1/5	1/3	1	3	5	7	9

Legend: Extr = Extremely; VStr = Very Strongly; Str = Strongly; Mod = Moderately.

simultaneously, with each component assigned a score based on its influence on groundwater occurrence in the region. The opinions of experts, combined with the researchers' understanding of the study area, were used to derive the aquifer hydraulic parameters presented in Table 5, as referenced by *Adiat et al. (2013)*. The results from Table 5 were then used to determine the relative weights of the groundwater prediction conditioning factors (GWPCFs) listed in Table 6. The consistency ratio was determined using the mathematical formulae from Eqs. (6) and (7), as established by *Zhou and Chen (2014)*.

$$\mathrm{CI} = \frac{\lambda_{max} - n}{n - 1}\,, \tag{5}$$

where CI is the consistency index, λ_{max} is the mean value of the consistency vector and n is the number of factors ($n = 4$).

$$\mathrm{CI} = \frac{4.129893 - 4}{4 - 1} = \frac{0.129893}{3} = 0.043298\,.$$

$$\mathrm{CR} = \frac{\mathrm{CI}}{\mathrm{RI}}\,, \tag{6}$$

where CR is the consistency ratio; RI is the random index, RI = 0.90 (*Wind and Saaty, 1980*).

$$\mathrm{CR} = \frac{0.043298}{0.9} = 0.043\,.$$

Inequality $0.043 < 0.1$ is consistent, as supported by *Feizizadeh et al. (2014)*. The weights generated are allocated to groundwater parameters (Table 7) to generate the groundwater prediction map. The mathematical algorithm for the groundwater prediction modelling index (GWPMI) is stated below:

$$\mathrm{GWPMI} = \mathrm{Tr}_W\,\mathrm{Tr}_R + \mathrm{K}_W\,\mathrm{K}_R + \mathrm{T}_W\,\mathrm{T}_R + \mathrm{L}_W\,\mathrm{L}_R\,, \tag{7}$$

where Tr represents the transverse resistance, K represents the hydraulic conductivity, T represents the aquifer transmissivity, and L represents the lineament density. The subscripts W and R are the normalised weights and ratings assigned to every groundwater prediction modelling index GWPMI parameter, respectively.

Table 6. Matrix of the pairwise, and the normalised weights for the thematic strata.

		Weighted Sum (Σ WS)	Normalised Weight (W)	Consistency Vector
Tr	$1(0.075)+1(0.091)+1/5(0.269)+1/7(0.565)$ $=0.2989$	0.299	0.075	$0.299/0.075=3.99$
K	$1(0.075)+1(0.091)+1/3(0.269)+1/5(0.565)$ $=0.3677$	0.368	0.091	$0.367/0.091=4.04$
T	$5(0.075)+3(0.091)+1(0.269)+1/3(0.565)$ $=1.10345$	1.103	0.269	$1.103/0.69=4.10$
L	$7((0.075)+5(0.091)+3(0.269)+1(0.565)$ $=2.352$	2.352	0.565	$2.35/0.565=4.16$

4.5. The modelling of the groundwater potentiality prediction model map

Table 7 presents the weights and ratings of the conditioning elements guiding groundwater potential in the investigated region. The groundwater potentiality prediction model (GWPM) map (Fig. 16) was developed in a spatial analysis environment, utilizing the categorization from columns 2 and 4 of Table 8. The GWPM map was created by dividing the GWPCFs maps into 36 grids and using the criteria map (Fig. 15) as a template to produce the groundwater prediction model map. The research area was classified into four possible zones: low, low-medium, medium, and medium-high (Fig. 16). The research site's middle regions and southern and northern peripheries possess modest groundwater potential. The northern and southern regions have low to medium groundwater potential. The eastern region has medium to high groundwater potential.

Table 8 illustrates the proportion of land included in each groundwater potential forecast zone. The results indicate values spanning from 3.2 to 13652.1. The 'low groundwater prospect regions' include an area of 83.36 km^2 (65%). The 'low-medium prospect regions' encompass an area

Table 7. Groundwater potentiality conditioning factor weights and ratings.

GWPCFs Parameters	**Classes**	**Groundwater Potentiality**	**Rating (R)**	**Normalised Weight (W)**
Transverse Resistance (Tr) (Ωm^2)	10.5 – 1050.8	Very low	1	0.075
	1050.9 – 1208.2	Low	2	
	1208.3 – 2248.6	Medium	3	
	2248.7 – 9127.3	Medium-high	4	
	9127.4 – 54807.4	High	5	
Hydraulic Conductivity (K) (m/day)	0.06 – 0.24	Very low	1	0.091
	0.25 – 0.26	Low	2	
	0.27 – 0.45	Medium	3	
	0.46 – 1.82	Medium-high	4	
	1.83 – 12.20	High	5	
Aquifer Transmissivity (T) (m^2/day)	0.0007 – 1.5	Very low	1	0.269
	1.6 – 1.8	Low	2	
	1.9 – 3.2	Medium	3	
	3.3 – 10.3	Medium-high	4	
	10.4 – 44.4	High	5	
Lineament Density (L)	0 – 0.0061	Very low	1	0.565
	0.00061 – 0.00121	Low	2	
	0.00121 – 0.00182	Medium	3	
	0.00182 – 0.00242	Medium High	4	
	0.00242 – 0.00302	High	5	

of 34.59 km^2 (27%). The 'medium prospective regions' include an area of 9.2 km^2 (7%). The medium- to high-prospect regions encompass an area of 1.27 km^2 (1%). This result is shown in the pie chart in Fig. 17. The analysis reveals that the investigated area is mainly occupied by poor potential zones (low to low-medium prospect regions) (92%).

Table 8. The groundwater prediction classification with the area covered in percentage.

Groundwater Potential Prediction Zones	Range	Area Covered (km^2)	Percentage Covered (%)
Low	3.2 – 650.5	83.36248	64.87353
Low-medium	650.5 – 1950.9	34.59804	26.92455
Medium	1950.9 – 4797.7	9.233134	7.185319
Medium-high	4797.7 – 13652.1	1.269171	0.987681

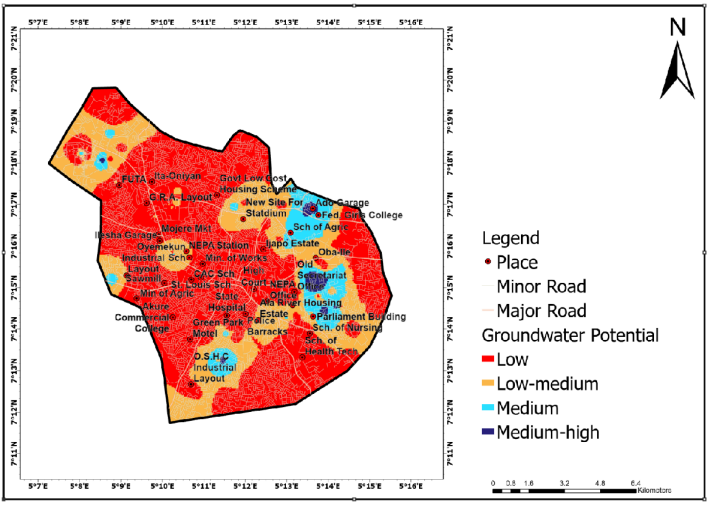

Fig. 16. Groundwater Prediction map of Akure metropolis.

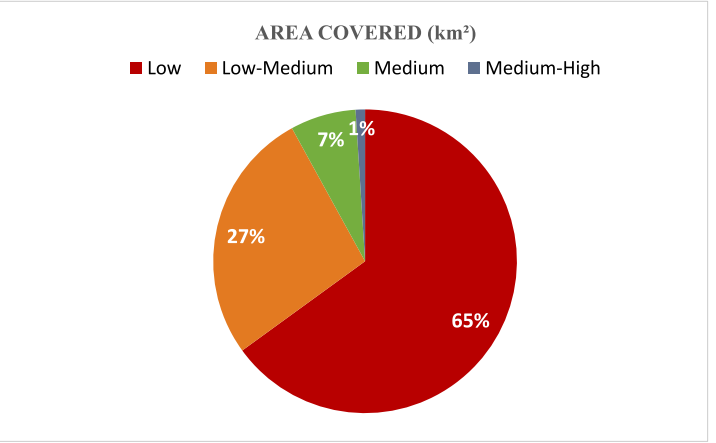

Fig. 17. Pie chart showing the area covered by the groundwater prediction map.

5. Conclusion

This study integrated ER survey and satellite imagery analysis to construct a comprehensive groundwater resource mapping framework for hydrological applications. The study utilised the VES data acquired to generate tables

and maps. The results from the iso-resistivity map of the saprolite layer have resistivity results between 6.1 and 1960.1 Ωm. The isopach map of the saprolite layer shows layer thickness values from 1.2 to 112 m. The depth to basement surface layer map has values between 2.6 to 147 m. The extracted data was then modified in geospatial analysis to generate the groundwater prediction model (GWPPM) map for the investigated area. The developed groundwater potential prediction model map demarcated the region into four different prediction zones of low, low-medium, medium and medium-high to effectively enhance the water resource in the region. The finalised groundwater distribution model reveals that approximately 92% of the metropolitan area exhibits limited resource capacity, with merely 8% demonstrating favourable extraction conditions. These findings demonstrate the spatial model's robust predictive capabilities and provide foundational knowledge for implementing sustainable groundwater management practices throughout the metropolitan region. The findings from the maps can guide borehole siting and help local water authority managers minimise borehole failures.

Declaration of conflict of interests. The authors declare no conflict of interest that could have influenced the work reported in this review.

Funding. No funding was sourced for this work.

Authors' contributions. All the authors drafted the manuscript and read and approved the final manuscript.

References

Abiola O., Enikanselu P., Oladapo M. I., 2009: Groundwater potential and aquifer protective capacity of overburden units in Ado-Ekiti, southwestern Nigeria. Int. J. Phys. Sci., **4**, 3, 120–132, doi: 10.5897/IJPS.9000285.

ACEP, 2006: Agro-Climatological and Ecological Project. Ministry of Agric. Fisheries and Forest Resources, Akure, Ondo State.

Adelusi A. O., 2009: Aquifer mapping and assessment of its risk using electrical resistivity sounding technique in Akure metropolis, southwestern Nigeria. Niger. J. Pure Appl. Phys., **4**, 65–73.

Ademilua O. L., Eluwole A. B., 2013: Hydrogeophysical Evaluation of the Groundwater Potential of Afe Babalola University Ado-Ekiti, Southwestern Nigeria. J. Emerg. Trends Eng. Appl. Sci., **4**, 1, 77–83.

Adeoye-Oladapo O. O., Mogaji K. A., Oladapo M. I., 2015: Multi-Array Hydro-Geoelectric Characterization of a Crystalline Basement Complex Environment. Phys. Sci. Int. J., **8**, 2, 1–18, doi: 10.9734/PSIJ/2015/17444.

Adepelumi A. A., Yi M.-J., Kim J.-H., Ako B. D., Son J. S., 2006: Integration of surface geophysical methods for fracture detection in crystalline bedrocks of southwestern Nigeria. Hydrogeol. J., **14**, 7, 1284–1306, doi: 10.1007/s10040-006-0051-2.

Adiat K. A. N., Nawawi M. N. M., Abdullah K., 2013: Application of Multi-Criteria Decision Analysis to Geoelectric and Geologic Parameters for Spatial Prediction of Groundwater Resources Potential and Aquifer Evaluation. Pure Appl. Geophys., **170**, 3, 453–471, doi: 10.1007/s00024-012-0501-9.

Aladejana O. O., Anifowose A. Y. B., Fagbohun B. J., 2016: Testing the ability of an empirical hydrological model to verify a knowledge-based groundwater potential zone mapping methodology. Model. Earth Syst. Environ., **2**, 4, 1–17, doi: 10.1007/s40808-016-0234-3.

Ayuk M. A., Adelusi A. O., Adiat K. A. N., 2013: Evaluation of groundwater potential and aquifer protective capacity assessment at Tutugbua-Olugboyega area, off Ondo road, Akure Southwestern Nigeria. Int. J. Phys. Sci., **8**, 1, 37–50, Academic Journals, doi: 10.5897/IJPS09.299.

Bello M. A., Oladapo M. I., Abraham-A. M. R., Orji O. M., 2025: Aquifer integrity test using the Dar Zarouk parameters in Emure Ekiti Southwestern Nigeria. Res. Earth Sci., **3**, 100087, doi: 10.1016/j.rines.2025.100087.

Biswas A., Jana A., Sharma S. P., 2012: Delineation of Groundwater potential zones using Remote Sensing and Geographic Information System Techniques: A case study from Ganjam district, Orissa, India. Res. J. Recent Sci., **1**, 9, 59–66.

Biswas A., Jana A., Mandal A., 2013: Application of remote sensing, GIS and MIF technique for elucidation of groundwater potential zones from a part of Orissa coastal tract, Eastern India. Res. J. Recent Sci., **2**, 11, 42–49.

Chowdhury A., Jha M. K., Chowdary V. M., Mal B. C., 2009: Integrated remote sensing and GIS-based approach for assessing groundwater potential in West Medinipur district, West Bengal, India. Int. J. Remote Sens., **30**, 1, 231–250, Taylor & Francis, doi: 10.1080/01431160802270131.

Edet A. E., Teme S. C., Okereke C. S., Esu E. O., 1996: Lineament analysis for groundwater exploration in Precambrian Oban Massif and Obudu Plateau, SE Nigeria. Int. J. Rock Mech. Min. Sci. Geomech. Abstr., **33**, 5, 215A, 965191, doi: 10.1016/0148-9062(96)80014-3.

Ekwe A. C., Onu N. N., Onuoha K. M., 2006: Estimation of aquifer hydraulic characteristics from electrical sounding data: the case of middle Imo River basin aquifers, south-eastern Nigeria. J. Spat. Hydrol., **6**, 2, 121–132.

Eluwole A. B., Olaolorun O. A., Ademilua O. L., Talabi A. O., Aturamu A. O., Ajisafe Y. C., Ojo O. F., Ajayi C. A., 2020: Subsurface electrical resistivity modelling over a suspected fault zone at Ojirami, Southwestern Nigeria. Model. Earth Syst. Environ., **6**, 4, 2543–2551, doi: 10.1007/s40808-020-00848-0.

Feizizadeh B., Blaschke T., Nazmfar H., 2014: GIS-based ordered weighted averaging and Dempster–Shafer methods for landslide susceptibility mapping in the Ur-

mia Lake Basin, Iran. Int. J. Digit. Earth, **7**, 8, 688–708, Taylor & Francis, doi: 10.1080/17538947.2012.749950.

Fitterman D. V., Deszcz-Pan M., Prinos S. T., 2012: Helicopter electromagnetic survey of the Model Land Area, Southeastern Miami-Dade County, Florida. Open-File Rep., 2012-1176, U.S. Geological Survey, 77 p., doi: 10.3133/ofr20121176.

Gupta D. S., Biswas A., Ghosh P., Rawat U., Tripathi S., 2022: Delineation of groundwater potential zones, groundwater estimation and recharge areas from Mahoba district of Uttar Pradesh, India. Int. J. Environ. Sci. Technol., **19**, 12, 12145–12168, doi: 10.1007/s13762-021-03795-0.

Hinnell A. C., Ferré T. P. A., Vrugt J. A., Huisman J. A., Moysey S., Rings J., Kowalsky M. B., 2010: Improved extraction of hydrologic information from geophysical data through coupled hydrogeophysical inversion. Water Resour. Res., **46**, 4, W00D40, doi: 10.1029/2008WR007060.

Ishola K. S., Fatoyinbo A. A., Hamid-Mosaku A. I., Okolie C. J., Daramola O. E., Lawal T. O., 2023: Groundwater potential mapping in hard rock terrain using remote sensing, geospatial and aeromagnetic data. Geosyst. Geoenviron., **2**, 1, 100107, doi: 10.1016/j.geogeo.2022.100107.

Jaafarzadeh M. S., Tahmasebipour N., Haghizadeh A., Pourghasemi H. R., Rouhani H., 2021: Groundwater recharge potential zonation using an ensemble of machine learning and bivariate statistical models. Sci. Rep., **11**, 1, 5587, Nature Publishing Group, doi: 10.1038/s41598-021-85205-6.

Joleha, Handayani Y. L., Sutikno S., Yusa M., 2024: Identification of potential groundwater zone for urban development. IOP Conf. Ser. Earth Environ. Sci., **1416**, 1, 012029, IOP Publishing, doi: 10.1088/1755-1315/1416/1/012029.

Kagabu M., Shimada J., Delinom R., Nakamura T., Taniguchi M., 2013: Groundwater age rejuvenation caused by excessive urban pumping in Jakarta area, Indonesia. Hydrol. Process., **27**, 18, 2591–2604, John Wiley & Sons, Ltd, doi: 10.1002/hyp.9380.

Kaliraj S., Chandrasekar N., Magesh N. S., 2014: Identification of potential groundwater recharge zones in Vaigai upper basin, Tamil Nadu, using GIS-based analytical hierarchical process (AHP) technique. Arab. J. Geosci., **7**, 4, 1385–1401, doi: 10.1007/s12517-013-0849-x.

Karim H. H., Schanz T., Ibrahim A. N., 2013: Integration between Surface Geoelectrical and Geotechnical Datasets in Salah Al-DinArea, Central Iraq?. Eng. Tech. J., **31**, A20, 237–261, doi: 10.30684/etj.2013.83798.

Khan A. A., Akhter S. H., Ahmed K. M., Hasan M. A., 2002: VES signature in soft rock groundwater exploration vis-à-vis geoenvironmental implications. In: Sherif M. M., Singh V. P., Al-Rashed M. (Eds.): Groundwater Hydrology (Vol. 2), Proceedings of the International Conference on Water Resources Management in Arid Regions (WRMiAR), A. A. Balkema Publishers, Leiden, pp. 179–193.

Kooy M., 2014: Developing informality: The production of Jakarta's urban waterscape. Water Altern., **7**, 1, 35–53.

Kumar P., Tiwari P., Biswas A., Acharya T., 2020: Geophysical and hydrogeological investigation for the saline water invasion in the coastal aquifers of West Bengal,

India: A critical insight in the coastal saline clay-sand sediment system. Environ. Monit. Assess., **192**, 9, 562, doi: 10.1007/s10661-020-08520-x.

Kumar P., Tiwari P., Singh A., Biswas A., Acharya T., 2021: Electrical Resistivity and Induced Polarization signatures to delineate the near-surface aquifers contaminated with seawater invasion in Digha, West-Bengal, India. Catena, **207**, 105596, doi: 10.1016/j.catena.2021.105596.

Kumar P., Tiwari P., Biswas A., Acharya T., 2023: Geophysical investigation for seawater intrusion in the high-quality coastal aquifers of India: a review. Environ. Sci. Pollut. Res., **30**, 4, 9127–9163, doi: 10.1007/s11356-022-24233-9.

Kumar P., Gupta D. S., Rao K., Biswas A., Ghosh P., 2024: Delineation of groundwater potential zones and its extent of contamination from the hard rock aquifers in West Bengal, India. Environ. Res., **249**, 118332, 1–24, doi: 10.1016/j.envres.2024.118332.

Madhav S., Singh P., 2021: Groundwater Geochemistry: Pollution and Remediation Methods. Wiley-Blackwell, 448 p.

Mallick J., Khan R. A., Ahmed M., Alqadhi S. D., Alsubih M., Falqi I., Hasan M. A., 2019: Modeling Groundwater Potential Zone in a Semi-Arid Region of Aseer Using Fuzzy-AHP and Geoinformation Techniques. Water, **11**, 12, 2656, Multidisciplinary Digital Publishing Institute, doi: 10.3390/w11122656.

Mogaji K. A., 2017: Development of AHPDST Vulnerability Indexing Model for Groundwater Vulnerability Assessment Using Hydrogeophysical Derived Parameters and GIS Application. Pure Appl. Geophys., **174**, 4, 1787–1813, doi: 10.1007/s00024-017-1499-9.

Mogaji K. A., Olayanju G. M., Oladapo M. I., 2011: Geophysical evaluation of rock type impact on aquifer characterization in the basement complex areas of Ondo State, Southwestern Nigeria: Geo-electric assessment and Geographic Information Systems (GIS) approach. Int. J. Water Resour. Environ. Eng., **3**, 4, 77–86.

Mogaji K. A., Lim H. S., Abdullah K., 2014: Modeling groundwater vulnerability prediction using geographic information system (GIS)-based ordered weighted average (OWA) method and DRASTIC model theory hybrid approach. Arab. J. Geosci., **7**, 12, 5409–5429, doi: 10.1007/s12517-013-1163-3.

Mogaji K. A., 2016a: Geoelectrical parameter-based multivariate regression borehole yield model for predicting aquifer yield in managing groundwater resource sustainability. J. Taibah Univ. Sci., **10**, 4, 584–600, doi: 10.1016/j.jtusci.2015.12.006.

Mogaji K. A., 2016b: Combining geophysical techniques and multi-criteria GIS-based application modeling approach for groundwater potential assessment in southwestern Nigeria. Environ. Earth Sci., **75**, 16, 1181, doi: 10.1007/s12665-016-5897-6.

Mogaji K. A., Omobude O. B., 2017: Modeling of geoelectric parameters for assessing groundwater potentiality in a multifaceted geologic terrain, Ipinsa Southwest, Nigeria – A GIS-based GODT approach. NRIAG J. Astron. Geophys., **6**, 2, 434–451, doi: 10.1016/j.nrjag.2017.07.001.

Neshat A., Pradhan B., Pirasteh S., Shafri H. Z. M., 2014: Estimating groundwater vulnerability to pollution using a modified DRASTIC model in the Kerman agricul-

tural area, Iran. Environ. Earth Sci., **71**, 7, 3119–3131, doi: 10.1007/s12665-013-2690-7.

Niaz A., Khan M. R., Mustafa S., Hameed F., 2016: Determination of aquifer properties and vulnerability mapping by using geoelectrical investigation of parts of Sub-Himalayas, Bhimber, Azad Jammu and Kashmir, Pakistan. Q. J. Eng. Geol. Hydrogeol., **49**, 1, 36–46, The Geological Society of London, doi: 10.1144/qjegh2015-070.

Nigerian Geological Survey Agency (Establishment) Act, 2006: Federal Republic of Nigeria.

Oborie E. L., Udom G. J., 2014: Determination of aquifer transmissivity using geoelectrical sounding and pumping test in parts of Bayelsa State, Nigeria. Peak J. Phys. Environ. Sci. Res., **2**, 2, 32–40.

O'Leary D. W., Friedman J. D., Pohn H. A., 1976: Lineament, linear, lineation: Some proposed new standards for old terms. Geol. Soc. Am. Bull., **87**, 10, 1463–1469, doi: 10.1130/0016-7606(1976)87<1463:LLLSPN>2.0.CO;2.

Olorunfemi M. O., Fasuyi S. A., 1993: Aquifer types and the geoelectric/hydrogeologic characteristics of part of the central basement terrain of Nigeria (Niger State). J. Afr. Earth Sci. Middle East, **16**, 3, 309–317, doi: 10.1016/0899-5362(93)90051-Q.

Oluyide P. O., 1988: Structural trends in the Nigerian basement complex. In: Oluyide P. O., Mbonu W. C., Ogezi A. E., Egbuniwe I. G., Ajibade A. C., Umeji A. C. (Eds.): Precambrian Geology of Nigeria. Geological Survey of Nigeria, Kaduna, pp. 93–98.

Omotola O. O., Oladapo M. I., Akintorinwa O. J., Mogaji K. A., 2019: Development of DRASTICLYS model for groundwater vulnerability assessment in the Akure Metropolis. Int. J. Eng. Sci. Technol., **11**, 8, 54–79.

Omotola O. O., Oladapo M. I., Akintorinwa O. J., 2020: Modeling assessment of groundwater vulnerability to contamination risk in a typical basement terrain case of vulnerability techniques application comparison study. Model. Earth Syst. Environ., **6**, 3, 1253–1280, doi: 10.1007/s40808-020-00720-1.

Pajock J., Gunalan J., Jothimani M., Abebe A., 2023: Assessment of groundwater potential zones using an integration of Remote Sensing, GIS and 2D Electrical Resistivity imaging in the Echway watershed, Baro River Basin, Southwest Ethiopia. IOP Conf. Ser. Mater. Sci. Eng., **1282**, 1, 012012, IOP Publishing, doi: 10.1088/1757-899X/1282/1/012012.

Paul R. S., Rawat U., SenGupta D., Biswas A., Tripathi S., Ghosh P., 2020: Assessment of groundwater potential zones using multi-criteria evaluation technique of Paisuni River Basin from the combined state of Uttar Pradesh and Madhya Pradesh, India. Environ. Earth Sci., **79**, 13, 340, doi: 10.1007/s12665-020-09091-3.

Richey A. S., Thomas B. F., Lo M.-H., Reager J. T., Famiglietti J. S., Voss K., Swenson S., Rodell M., 2015: Quantifying renewable groundwater stress with GRACE. Water Resour. Res., **51**, 7, 5217–5238, doi: 10.1002/2015WR017349.

Salako A. O., Osotuyi A. G., Adepelumi A. A., 2019: Seepage investigations of heterogeneous soils beneath some buildings using geophysical approaches: example from southwestern Nigeria. Int. J. Geo-Eng., **10**, 1, 11, doi: 10.1186/s40703-019-0107-5.

Sattar G. S., Keramat M., Shahid S., 2016: Deciphering transmissivity and hydraulic conductivity of the aquifer by vertical electrical sounding (VES) experiments in Northwest Bangladesh. Appl. Water Sci., **6**, 1, 35–45, doi: 10.1007/s13201-014-0203-9.

Sharma S. P., Biswas A., 2013: A practical solution in delineating thin conducting structures and suppression problem in direct current resistivity sounding. J. Earth Syst. Sci., **122**, 4, 1065–1080, doi: 10.1007/s12040-013-0327-6.

Sikah J., Aning A., Danuor S., Manu E., Okrah C., 2016: Groundwater Exploration using 1D and 2D Electrical Resistivity Methods. J. Environ. Earth Sci., **6**, 7, 55–63.

Singh K. P., 2005: Nonlinear estimation of aquifer parameters from surficial resistivity measurements. Hydrol. Earth Syst. Sci. Discuss., **2**, 917–938, doi: 10.5194/hessd-2-917-2005.

Singh S., Gautam P. K., Kumar P., Biswas A., Sarkar T., 2021: Delineating the characteristics of saline water intrusion in the coastal aquifers of Tamil Nadu, India by analyzing the Dar-Zarrouk parameters. Contrib. Geophys. Geod., **51**, 2, 141–163, doi: 10.31577/congeo.2021.51.2.3.

Stigter T. Y., Ribeiro L., Carvalho Dill A. M. M., 2006: Evaluation of an intrinsic and a specific vulnerability assessment method in comparison with groundwater salinisation and nitrate contamination levels in two agricultural regions in the south of Portugal. Hydrogeol. J., **14**, 1-2, 79–99, Springer, doi: 10.1007/s10040-004-0396-3.

Ugada U., Ibe K. K., Akaolisa C. Z., Opara A. I., 2014: Hydrogeophysical evaluation of aquifer hydraulic characteristics using surface geophysical data: a case study of Umuahia and environs, Southeastern Nigeria. Arab. J. Geosci., **7**, 12, 5397–5408, doi: 10.1007/s12517-013-1150-8.

Wind Y., Saaty T. L., 1980: Marketing Applications of the Analytic Hierarchy Process. Manag. Sci., **26**, 7, 641–658, doi: 10.1287/mnsc.26.7.641.

Zhou L., Chen Y., 2014: Exploring the potential of community-based grassland management in Yanchi County of Ningxia Hui Autonomous Region, China: an application of the SWOT-AHP method. Environ. Earth Sci., **72**, 6, 1811–1820, doi: 10.1007/s12665-014-3090-3.